Materials Advances

ROYAL SOCIETY OF CHEMISTRY

PAPER

View Article Online
View Journal | View Issue

Cite this: *Mater. Adv.*, 2026, 7, 1089

Complexation-driven synthesis of potassium copper ferrocyanide nanoparticles for nonenzymatic glucose detection: an electrochemical and FET-based approach

Chandan Saha, Pooja Kumari, Mustafizur Hazarika and Kaushik Mallick *

The detection of glucose holds significant importance in clinical medicine, particularly for the diagnosis and management of diabetes. In this study, a complexation-mediated strategy was employed to synthesize nanostructured potassium copper ferrocyanide (PCFC) nanoparticles within the size range of 2 to 5 nm, which were subsequently investigated for their potential application in non-enzymatic electrochemical and field-effect transistor-based glucose sensing platforms. Key performance metrics of the sensor, including sensitivity, detection limit, linear response range, response time and selectivity towards glucose in an alkaline electrolyte medium, were systematically investigated. Electrochemical measurements, utilizing cyclic voltammetry (CV) and differential pulse voltammetry (DPV), confirmed the electrocatalytic activity of the synthesized material for glucose oxidation, primarily attributed to the crucial role of the Cu^{2+}/Cu^{3+} redox couple. The CV and DPV techniques yielded sensitivities of 0.41 mA mM^{-1} cm^{-2} and 0.50 mA mM^{-1} cm^{-2}, with limits of detection of 1.09 mM and 1.01 mM, respectively. Application of potassium copper ferrocyanide within an extended gate-field effect transistor architecture showed promising glucose sensing performance, as evidenced by linear shifts in transfer characteristics and effective modulation of drain current upon glucose addition, with the sensitivity and limit-of-detection values of 0.033 mA mM^{-1} cm^{-2} and 0.28 mM, respectively. The sensor exhibited good sensitivity, a low detection limit and excellent selectivity in the presence of common biological interferents. The practical applicability of the transistor-based sensor was also demonstrated through real-sample analysis, which showed high accuracy and repeatability, suggesting its potential for practical biomedical and clinical diagnostic applications.

Received 10th September 2025,
Accepted 2nd December 2025

DOI: 10.1039/d5ma01041a

rsc.li/materials-advances

1. Introduction

Diabetes mellitus is a chronic metabolic disorder marked by persistently elevated blood glucose levels, primarily caused by insufficient insulin production. Prolonged diabetes can result in a variety of severe health complications, including vision impairment or blindness due to diabetic retinopathy, cardiovascular diseases and chronic kidney failure.[1] Therefore, it is essential to monitor and effectively regulate blood glucose levels to prevent complications and ensure optimal disease management in individuals with diabetes. For this reason, extensive research activities have been dedicated to the advancement of glucose sensors, with a particular focus on their application in the early detection, diagnosis and management.[2] Accurate measurement of glucose concentration is not only crucial for medical applications but also plays a significant role in various fields such as pharmaceutical drug synthesis, environmental monitoring and quality control in food analysis.[3]

Currently, a wide range of techniques, such as optical, electrochemical and microwave sensing methods, have been developed and refined for effective detection and quantification of glucose in various applications.[4–6] Among the various types of sensing technologies, electrochemical sensors have attracted significant attention due to their high sensitivity, rapid response time, low detection limits, broad linear detection range and cost-effective fabrication, making them suitable for practical applications.[7] Electrochemical glucose sensors are categorized into enzyme-based and enzyme-free types, each offering distinct mechanisms for glucose detection and varying in terms of sensitivity, stability and fabrication complexity.[8] Traditionally, glucose concentration was measured using enzyme-based methods known for high selectivity but limited by complex enzyme handling, temperature and low sensitivity from indirect electron transfer.[9–11] Therefore, enzyme-free

Department of Chemical Sciences, University of Johannesburg, P.O. Box: 524, Auckland Park, 2006, South Africa. E-mail: kaushikm@uj.ac.za

glucose sensors offer a promising alternative by addressing the inherent limitations of enzyme-based systems, providing enhanced stability, lower production costs and more reliable performance under varying environmental conditions.[5,12,13]

In addition to conventional electrochemical glucose sensors, field-effect transistor (FET)-based glucose sensors have emerged as a compelling alternative due to their highly sensitive semiconducting channels, which offer superior detection capabilities compared to standard sensors, such as glucometers. These sensors are particularly advantageous for continuous and real-time glucose monitoring. Their compatibility with miniaturized, low-power electronic systems makes them highly suitable for integration into portable, wearable or even implantable devices.[14] The growing demand for non-invasive, real-time health monitoring technologies has further motivated the development of FET-based glucose sensors, positioning them as a next-generation solution for effective diabetes management and personalized healthcare.[15,16] Ion-sensitive field-effect transistors, a type of MOSFET with the metal gate replaced by an ion-sensitive platform, are widely used for detecting ions and molecules due to their internal gain and CMOS compatibility.[17,18] They have been applied in various biomedical sensors, including those for pH, glucose and cholesterol.[19–21] However, ion-sensitive transistors face challenges such as high noise and limited stability under harsh conditions. To address these issues, extended-gate FETs have been developed, where the sensing electrode is separated from the transistor. This design improves durability and simplifies fabrication by isolating the transistor from chemical exposure.

Different sensing electrodes are required to detect a wide range of analytes, as each target demands a specific interface for selective and efficient recognition. Optimized performance depends on fabricating electrodes using techniques tailored to the physicochemical properties and the sensing requirements of the materials. Careful control of surface morphology, conductivity, catalytic activity and chemical affinity is essential to achieve high sensitivity, stability and reproducibility, enabling robust electrode platforms for accurate and reliable detection across diverse conditions. A variety of advanced materials, including carbon-based materials and metal oxides, have been used as glucose sensing platforms due to their excellent electrical properties, high surface area and remarkable biocompatibility.[20–25]

In this work, we present a facile and straightforward complexation-based synthesis strategy for producing hexane-1,6-diamine-stabilized, nanostructured potassium copper ferrocyanide (PCFC) particles. The approach enables the controlled formation of highly uniform nanoparticles that crystallize in a well-defined face-centered cubic (FCC) structure, exhibiting a narrow size distribution in the range of approximately 2–5 nm. This method not only ensures excellent structural homogeneity but also provides improved stability and dispersibility due to effective surface coordination by hexane-1,6-diamine. The electrocatalytic properties of the synthesized copper ferrocyanide were thoroughly evaluated for its application in both non-enzymatic electrochemical and field-effect transistor-based nonenzymatic glucose sensing platforms. Key performance metrics of the fabricated glucose sensor were systematically studied, including its sensitivity, detection limit, linear response range, response time and selectivity toward glucose in an alkaline electrolyte medium.

2. Experimental

2.1. Materials

This study utilized analytical grade copper nitrate, potassium ferrocyanide, hexane-1,6-diamine (HMDA), dopamine, epinephrine, sucrose, cholesterol and glucose from Sigma Aldrich. Indium tin oxide (ITO) coated glass and Fusayama/Meyer artificial saliva solution were received from Sigma Aldrich.

2.2. Synthesis of organic molecule stabilized potassium copper ferrocyanide (PCFC) nanoparticles

To synthesize potassium copper ferrocyanide (PCFC), a stepwise chemical procedure was followed. Initially, 0.10 g of HMDA was dissolved in 10 mL of methanol under continuous stirring to ensure complete dissolution. In the subsequent step, 3 mL of a 0.1 M aqueous potassium ferrocyanide solution was added dropwise under stirring conditions to the diamine-containing methanolic solution. This addition led to the formation of a white precipitate, which was preliminarily identified as a ferrocyanide–HMDA complex, suggesting an interaction between the amine groups and the ferrocyanide ions. After the formation of the white precipitate, 4 mL of copper sulphate solution (0.1 M) was added directly to the reaction mixture. As a result, a distinct perylene maroon coloration was developed, which indicated the formation of PCFC (Scheme 1). The resulting solid product was then separated from the reaction mixture by filtration to remove any unreacted materials and by-products. The filtered material was thoroughly dried under vacuum conditions to eliminate residual solvents, thereby yielding the final PCFC product in solid form.

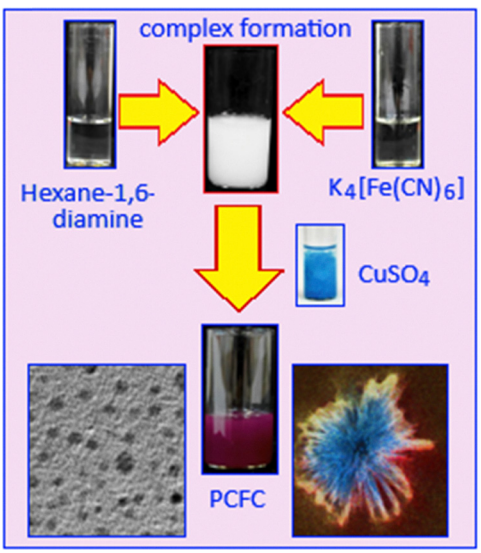

Scheme 1 Detailed synthesis steps for the formation of organic molecule stabilized potassium copper ferrocyanide (PCFC) nanoparticles.

The purified compound was subsequently subjected to a series of analytical characterization techniques, such as spectroscopy and microscopy, to confirm its composition and structure. Furthermore, the performance of PCFC was determined, as a glucose sensor, by analyzing parameters such as sensitivity, linear detection range, response time and detection limit.

2.3. Formulation of the PCFC-based active material as a catalyst

To modify the electrode, a catalyst slurry was prepared by dispersing 2.0 mg of PCFC in 100 μL of a methanol–Nafion mixture (10 : 1, v/v) and thoroughly mixing to achieve a uniform distribution of the PCFC particles.

2.4. Material analysis methods

To study the characteristics of the material, a variety of analytical techniques were employed for structural, morphological, spectroscopic and electrochemical evaluation. Crystallographic information, including phase composition, was obtained from X-ray diffraction (XRD) using a PANalytical X'pert instrument. Nanoscale structural details and morphology were examined through transmission electron microscopy (TEM, JEOL JEM-2100) and scanning electron microscopy (SEM, JEOL JSM-840), respectively. Spectroscopic analyses included Raman spectroscopy (Jobin-Yvon T64000 spectrometer) to probe vibrational properties and chemical bonding and X-ray photoelectron spectroscopy (XPS, Thermo Scientific MultiLab 2000) to analyse surface elemental composition and chemical states. The electrochemical behaviour of the catalyst was investigated using a Bio-Logic SP-300 potentiostat.

2.5. Electrochemical experiment

Electrochemical measurements were performed utilizing a standard three-electrode cell setup containing 6 mL of 0.1 M sodium hydroxide electrolyte. Within this electrolyte, a counter electrode (platinum wire), a reference electrode, Ag/AgCl (RE-1B), and a catalyst modified glassy carbon working electrode (GCE) were immersed. Prior to modification, the GCE surface was prepared through a standard cleaning procedure involving polishing with alumina on a microcloth, followed by rinsing with ethanol and drying under a heating lamp. Electrode modification was then achieved by dropcasting 10 μL of the PCFC catalyst ink onto the cleaned GCE surface and allowing it to dry.

2.6. Preparation of the PCFC modified ITO electrode for field-effect transistor studies

PCFC modified ITO electrodes were fabricated using a spin-coating technique. The process involved dispensing 40 μL of the PCFC ink onto the ITO surface, followed by a spinning operation at 2000 rpm for 150 seconds. This deposition and spinning cycle was carried out four times to build up a uniform layer of the material across the substrate. The PCFC deposited ITO electrodes were subjected to drying in a hot air oven at 80 °C.

3. Results and discussion

The reaction between potassium ferrocyanide and hexane-1,6-diamine (HMDA) leads to the formation of a ferrocyanide–HMDA complex, primarily due to the structural and chemical properties of HMDA. The amine groups in HMDA contain nitrogen atoms with lone pairs, allowing it to act as an effective ligand that coordinates with the ferrocyanide species forming a complex. Subsequent reaction of copper sulphate with this ferrocyanide–HMDA complex results in the formation of potassium copper ferrocyanide particles. Complexation plays a crucial role in enabling the formation of nanoparticles with uniform size and shape. In this system, HMDA serves as a stabilizing agent, preventing uncontrolled particle growth and aggregation.

X-ray diffraction analysis confirmed the successful formation of potassium copper ferrocyanide, $K_2Cu[Fe(CN)_6]$. The diffraction pattern (Fig. 1A) displayed prominent peaks at 15.2°, 17.78°, 25.21°, 35.31°, 39.76°, 44.52°, 52.31°, 56.16°, and 57.62°, corresponding to the (110), (200), (220), (440), (420), (422), (440), (660) and (620) crystallographic planes, respectively. These diffraction features are consistent with the JCPDS reference code 53-0084, corresponding to a face-centered cubic structure with a space group of $Fm\bar{3}m$. Fig. 1B shows the unit cell structure of potassium copper ferrocyanide, where copper and iron ions are octahedrally coordinated and interconnected *via* cyanide (C≡N) ligands, resulting in a three-dimensional framework.[26,27]

Fig. 2(A) and (B) display the transmission electron microscopy images of potassium copper ferrocyanide nanoparticles stabilized by hexane-1,6-diamine with different magnifications. These nanoparticles exhibit a narrow size distribution in the range of 2 to 5 nm, as quantitatively represented in the corresponding size distribution histogram (Fig. 2B, inset). In the TEM image, the dark spots correspond to the individual nanoparticles, which are uniformly and highly dispersed throughout the organic matrix. This high degree of dispersion indicates effective stabilization by the organic molecules, preventing particle aggregation. Fig. 3A shows the scanning electron microscopy image of the organic–inorganic hybrid system with a rosette-like aggregate indicating a directional growth mechanism. A higher magnification SEM image, Fig. 3B, reveals a complex arrangement of acicular crystals radiating from a central point, forming a densely packed core and a more

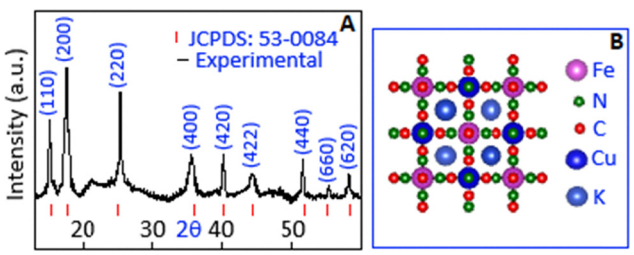

Fig. 1 (A) X-ray diffraction pattern and (B) unit cell representation of potassium copper ferrocyanide.

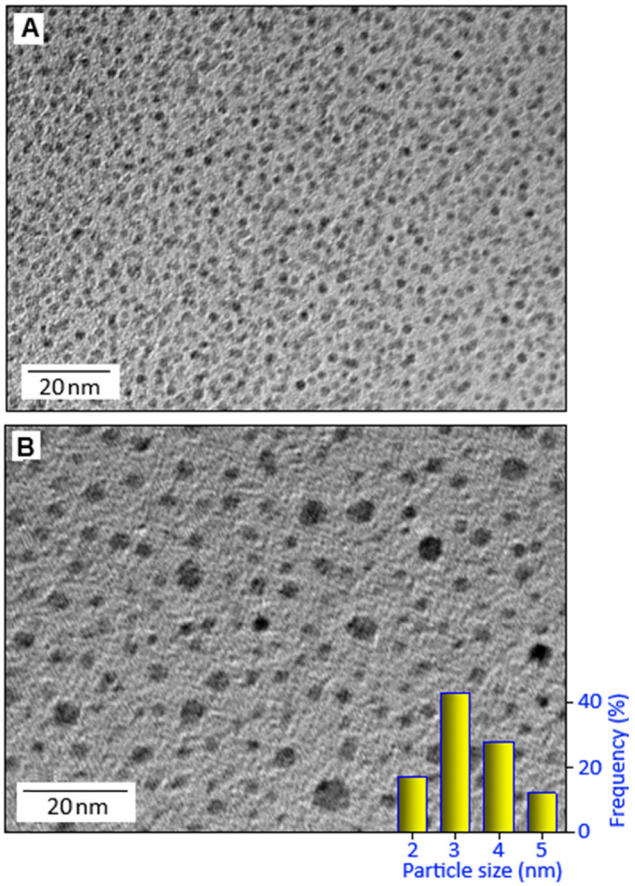

Fig. 2 (A) and (B) Transmission electron microscopy images of hexane-1,6-diamine stabilized potassium copper ferrocyanide nanoparticles and (inset of B) size distribution histogram.

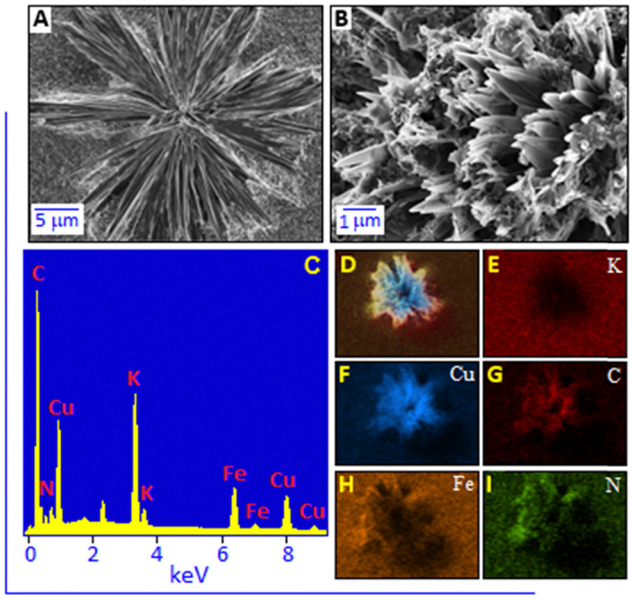

Fig. 3 (A) and (B) Scanning electron microscopy images of the organic–inorganic hybrid system with different magnifications. (C) Energy dispersive X-ray spectrum of potassium copper ferrocyanide. Elemental mapping of the overlapping image (D) and the distributions of K, Cu, C, Fe and N, (E)–(I), respectively, in potassium copper ferrocyanide.

dispersed periphery. The faceted surface of the individual crystals suggests a complex growth mechanism, contributing to the overall three-dimensional, flower-like morphology. Elemental analysis using the energy dispersive X-ray spectroscopy technique shows the presence of Cu, Fe, K, C and N in the sample, which correspond to the constituent elements of potassium copper ferrocyanide (Fig. 3C). The elemental mapping shows the overlapping image (Fig. 3D) and uniform distributions of K, Cu, C, Fe and N in PCFC (Fig. 3(E)–(I)). The elemental mapping also ensures well-integrated elements in potassium copper ferrocyanide at a microscopic level, without any significant segregation or uneven distribution of the components. Deconvoluted Raman spectra (Fig. 4A) exhibited the presence cyano group (–C≡N) in the range of 1800–2400 cm^{-1}. Two distinct peaks were observed at 2095 and 2140 cm^{-1}, corresponding to the stretching vibrations of the cyano group.[28] X-ray photoelectron spectroscopy analysis was employed to investigate the elemental composition and corresponding oxidation states of the constituent elements of potassium copper ferrocyanide. This surface-sensitive technique provides valuable insights into the chemical environment and bonding states by precisely measuring the binding energies of core-level electrons. The XPS survey spectrum (Fig. 4B, main panel) confirmed the presence of potassium, copper, iron, carbon and nitrogen, which is consistent with the expected elemental composition of $K_2Cu[Fe(CN)]_6$. High-resolution spectra were subsequently recorded for each element to determine their chemical states. The high-resolution K 2p spectrum (Fig. 4B, inset) shows the two prominent peaks positioned at 292.48 and 295.30 eV corresponding to K $2p_{1/2}$ and K $2p_{3/2}$, respectively.[29] The high resolution spectrum of Cu 2p (Fig. 4C) displays two main peaks at 935.6 and 955.7 eV matching with binding energies of Cu $2p_{3/2}$ and Cu $2p_{1/2}$, respectively, with a spin–orbit splitting separation of 20.1 eV, which is consistent with the literature.[30] These peaks are attributable to Cu(II) states. The presence of satellite peaks at 941.91 and 943.88 is a characteristic feature of Cu(II) species, confirming that copper exists in the +2-oxidation state within the structure.[31] The high-resolution Fe 2p spectrum, Fig. 4D, exhibits two major peaks at the binding energy values of 708.02 and 720.85 eV, corresponding to Fe $2p_{3/2}$ and Fe $2p_{1/2}$, respectively. This spectral signature provides evidence of the Fe(II) state within the sample.[32] Deconvolution of the C 1s, Fig. 4E, and N 1s, Fig. 4F, spectra resulted in two main peaks located at 284.36 and 397.34 eV, respectively, indicative of C–N bonding within the synthesized material.[32] In addition, two weak peaks at 285.08 and 399.61 eV, implying the defective C≡N sites, are present within Fe–CN–Cu bridges.[33]

3.1. Mechanistic role of the Cu^{2+}/Cu^{3+} redox couple in glucose oxidation

To elucidate the electrochemical mechanism underlying glucose oxidation in the presence of the PCFC catalyst, cyclic voltammetry (CV) measurements were performed at a scan rate

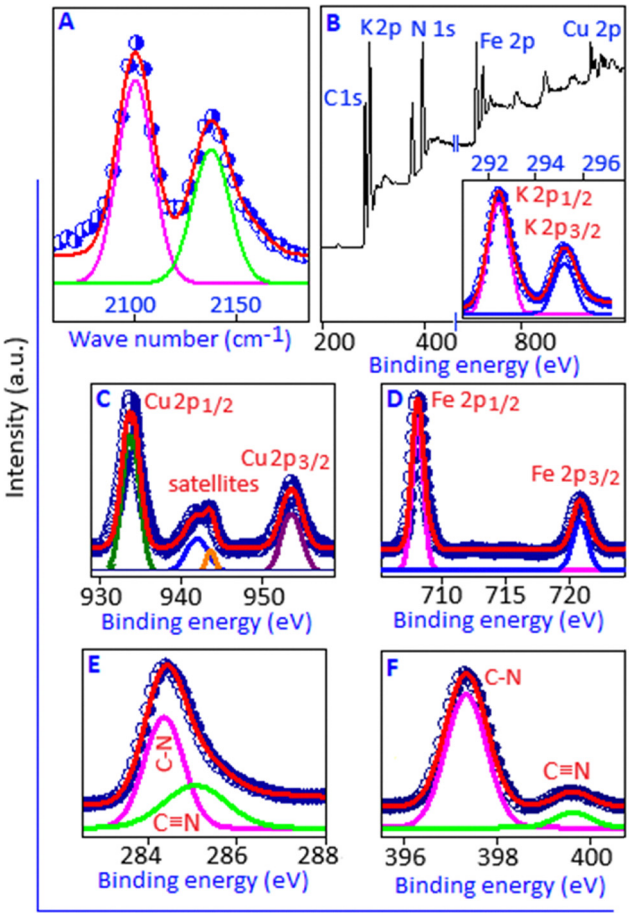

Fig. 4 (A) Raman spectrum of the cyano group, in the range of 1800–2400 cm^{-1}, with the peak positions at 2095 and 2140 cm^{-1}. (B) XPS survey spectrum of potassium copper ferrocyanide confirming the presence of K, Cu, Fe, C, and N. Inset: high-resolution K 2p spectrum. (C)–(F) High-resolution XPS spectrum of Cu 2p, Fe 2p, C 1s and N 1s.

of 50 mV s^{-1} in an alkaline medium consisting of 0.1 M NaOH. This electrochemical technique was employed to evaluate the redox behavior of the system, identify the potential at which glucose oxidation occurs, and assess the catalytic activity and electron transfer kinetics facilitated by PCFC. Sodium hydroxide electrolyte is widely utilized in non-enzymatic glucose sensing with copper-based materials, due to its ability to create an alkaline environment that promotes the redox transition of copper species.[5,34] The redox transition is essential for the catalytic oxidation of glucose, as it enables efficient electron transfer between the glucose molecules and the electrode surface, thereby enhancing the overall sensitivity and performance of the sensor.[35–37]

The CV scans, as illustrated in Fig. 5A, main panel, exhibit a distinct anodic signature within the potential window of 0.5 to 0.7 V upon the successive addition of glucose at concentrations ranging from 4 to 24 mM. The voltammogram characteristics indicate the occurrence of glucose oxidation facilitated by the electrocatalytic activity of the PCFC modified electrode. The progressive increase in peak current with rising glucose concentrations confirms the catalytic role of the electrode and the sensitivity of the system to glucose molecules. The inset of Fig. 5A demonstrates a clear linear relationship between the anodic peak current, measured at 0.7 V, and the glucose concentration. This linear trend indicates a proportional electrochemical response of the sensor. From the slope of the calibration curve, the sensitivity value of the sensor was determined to be 0.41 mA mM^{-1} cm^{-2}. Furthermore, the limit of detection (LOD) was calculated to be 1.09 mM, demonstrating the capability of the sensor to detect glucose at physiologically relevant concentrations.

It has been reported that a nonenzymatic glucose sensor based on nanoporous copper thin film exhibited the sensitivity value of 2.2 mA mM^{-1} cm^{-2} with a detection limit of 0.025 μM, in the range of 1 μM to 2 mM.[38] A Cu–Cu_2O nanocomposite modified electrode was employed for a highly selective non-enzymatic glucose biosensor, which exhibited a linear detection upper limit of 40 mM with a sensitivity value of 1434.12 μA cm^{-2} mM^{-1}.[39] An electrospinning-based fabrication method was reported for the development of a nanofibrous composite consisting of copper nanoflowers decorated on gold nanoparticle-functionalized graphene oxide for electrochemical glucose detection. The sensor exhibited an extended linear detection range from 0.001 to 0.1 mM and achieved a low detection limit of 0.018 μM, highlighting its potential for trace-level glucose monitoring.[40] A polydopamine-wrapped Cu–Cu(II) heterostructure was designed for a non-enzymatic glucose detecting system that exhibited a sensitivity value of 223.17 μA mM^{-1} cm^{-2} with a detection limit of 20 μM. The Cu-polydopamine-based sensor demonstrated excellent selectivity, reproducibility and long-term stability, along with effective applicability for glucose detection in human urine samples, indicating its potential for biomedical and clinical diagnostic applications.[41]

The abovementioned electrochemical findings are consistent with the widely accepted mechanism for non-enzymatic glucose sensing using copper-based materials under alkaline conditions.[8] The process involves the initial formation of $Cu(OH)_2$ on the electrode surface in the presence of NaOH electrolyte. During the application of a suitable anodic potential, Cu^{2+} is oxidized to Cu^{3+} (in the form of CuOOH). This higher-valence copper species then acts as a potent oxidizing agent, catalytically converting glucose to gluconolactone, Glu-L (which is further oxidized to gluconic acid), while Cu^{3+} is reduced back to Cu^{2+}. The continuous cycling between Cu^{2+} and Cu^{3+} states facilitates the electron transfer, resulting in the observed enhancement of the anodic current in the presence of glucose and confirming the central catalytic role of the Cu^{2+}/Cu^{3+} redox couple in the sensing mechanism.[8] In this study, the overlapped peaks observed around 0.5 V (Fig. 5A, main panel) correspond to the $Cu^{2+} \rightarrow Cu^{3+}$ transition that initiates the glucose oxidation.[5] The above mechanism of glucose detection by the PCFC electrocatalyst is shown in the following equations (1), (2) and (3):

$$Cu^{2+} + 2OH^- \rightarrow Cu(OH)_2 + 2e^- \quad (1)$$

$$Cu(OH)_2 + OH^- \rightarrow CuOOH + H_2O + e^- \quad (2)$$

$$CuOOH + Glucose \rightarrow Cu(OH)_2 + Gluconolactone \quad (3)$$

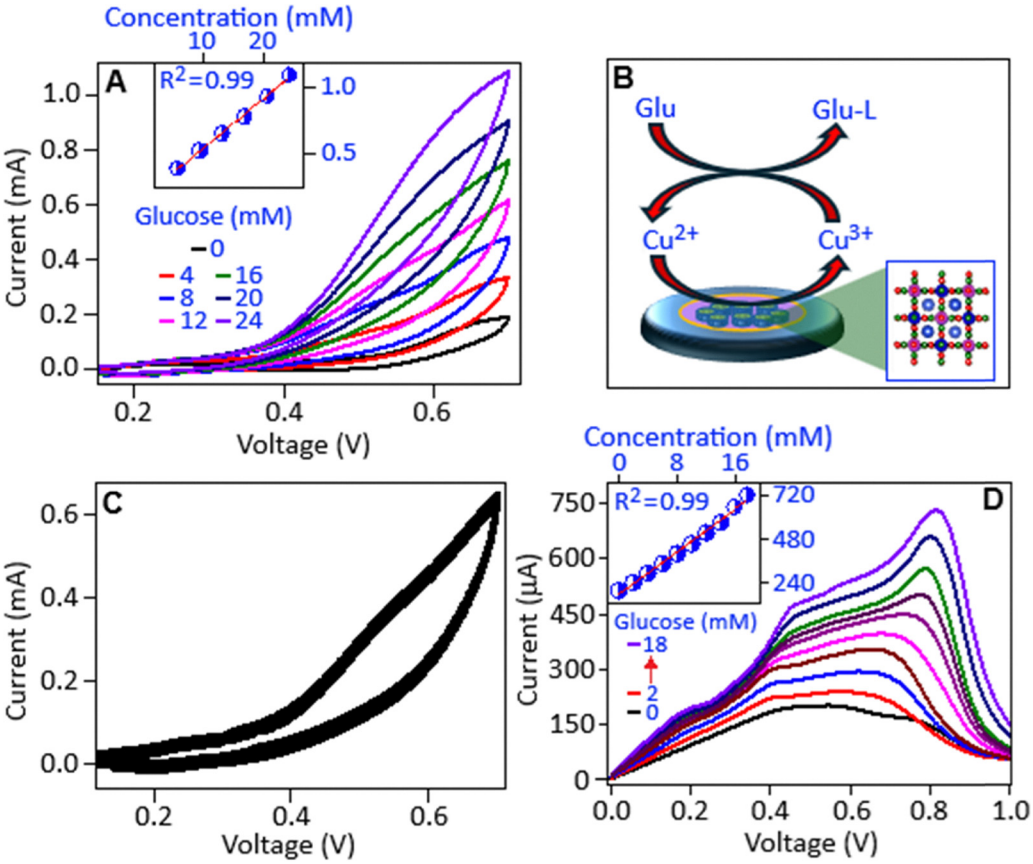

Fig. 5 (A) Cyclic voltammogram of the PCFC modified electrode in 0.1 M NaOH with increasing glucose concentrations (0–24 mM). The inset shows a linear relationship between anodic peak current and glucose concentration. (B) Schematic illustration of the non-enzymatic glucose sensing mechanism involving the Cu^{2+}/Cu^{3+} redox couple. (C) Long-term stability of the sensor assessed for 100 consecutive CV cycles. (D) Differential pulse voltammetry curves of the PCFC modified electrode with increasing glucose concentrations (2–18 mM). The inset shows the linear relationship between the DPV peak current and the glucose concentration.

The glucose oxidation mechanism and corresponding $Cu^{2+} \rightarrow Cu^{3+}$ transition are schematically represented in Fig. 5B. The operational stability of the electrocatalyst is a critical parameter for practical applications. Fig. 5C displays the long-term stability of the sensor which was assessed by performing 100 consecutive CV cycles in a solution containing 12 mM glucose in the presence of NaOH (0.1 M) electrolyte. The electrode demonstrated high stability, exhibiting a nominal decrease in current response after 100 cycles, suggesting robust catalytic performance of the PCFC-modified electrode over extended use.

Differential pulse voltammetry (DPV), a potentiostatic technique designed to minimize background charging currents and offering advantages over common methods like cyclic voltammetry, was also employed to further investigate the electrocatalytic performance of PCFC in glucose oxidation. The DPV results, Fig. 5D, showed a well-defined glucose oxidation peak centred at ~0.8 V within the concentration range of 2–18 mM. Consistent with the CV findings, the intensity of the DPV current peaks scaled linearly with increasing glucose concentration (Fig. 5D, inset). The sensitivity and LOD derived from the DPV measurements were 0.50 mA mM^{-1} cm^{-2} and 1.01 mM, respectively, further confirming the effective electrocatalytic activity of the PCFC based material towards glucose oxidation.

3.2. Glucose sensing performance using the extended gate-field effect transistor (EGFET)

The extended gate-field effect transistor (EGFET) architecture separates the sensing element from the gate, solving the limitations of ISFET, including instability and direct exposure of the gate dielectric to the analyte solution.[42–44] This configuration involves a standard MOSFET whose gate is electrically connected to an external sensing electrode (working electrode) immersed in the analyte solution. A reference electrode is also placed in the same solution, completing the electrochemical cell setup. The key advantage of the EGFET lies in the physical separation, which enhances chemical stability, simplifies packaging and allows versatile use of different materials for the sensing electrode tailored to specific analytes. The potential developed at the interface between the sensing electrode and the analyte within the electrolyte solution modulates the gate potential of the MOSFET.

For glucose sensing using an EGFET, the interaction occurs at the interface between the functionalized working electrode

(PCFC-coated ITO) and glucose molecules in the presence of the electrolyte (0.1 M NaOH). This interaction modifies the electrochemical potential at the electrode surface.[45–48] The change in surface potential contributes to the overall effective gate-source voltage experienced by the FET channel. The effective threshold voltage of the EGFET (V_{th_EGFET}) can be conceptualized as the MOSFET threshold voltage modified by the electrochemical potentials within the sensing setup as described in equation (4):

$$V_{th\_EGFET} \approx V_{th\_Mos} + V_{GS} + \chi_{Sol} - V_{ref} \quad (4)$$

Here, V_{th_Mos} represents the intrinsic threshold voltage of the MOSFET, V_{ref} represents the analyte-sensitive potential difference at the catalyst–electrolyte interface, V_{GS} is the applied potential on the gate and χ_{sol} is the surface dipole potential of the electrolyte. This relationship highlights the overall threshold voltage modulation of the sensor by the electrochemical environment established at the extended gate.[49]

The FET characterization was performed using a dual-channel Keithley source measurement unit configured for EGFET measurements, Fig. 6A. The setup involved grounding the source terminal of the n-type FET in the CD4007UB, while a potential was applied to the drain to establish the drain-source bias voltage (V_{DS}). The gate terminal was directly connected to the modified working electrode, forming the extended gate. Simultaneously, a controlled potential was applied *via* the measurement unit to the reference electrode immersed in the electrolyte solution, completing the electrochemical cell. The performance of the sensor was characterized through transfer characteristics, output characteristics and amperometric measurements. At low V_{DS} ($V_{DS} < V_{GS} - V_{th}$), I_{DS} exhibits a linear dependence on V_{DS}. The drain current is approximated using equation (5):

$$I_{Linear} = \mu \frac{W}{2L} C_{OX} \{2(V_{GS} - V_{th}) V_{DS} - V_{DS}^2\} \quad (5)$$

where V_{th} is the threshold voltage, μ is the charge carrier mobility, W/L is the channel aspect ratio, and C_{OX} is the gate oxide capacitance per unit area.

Transfer characteristics (I_{DS}–V_{GS}), recorded at a constant drain voltage of 0.1 V, Fig. 6B, demonstrated the sensing response as increasing glucose concentration (0–10 mM) progressively shifted the curves toward higher gate voltages,

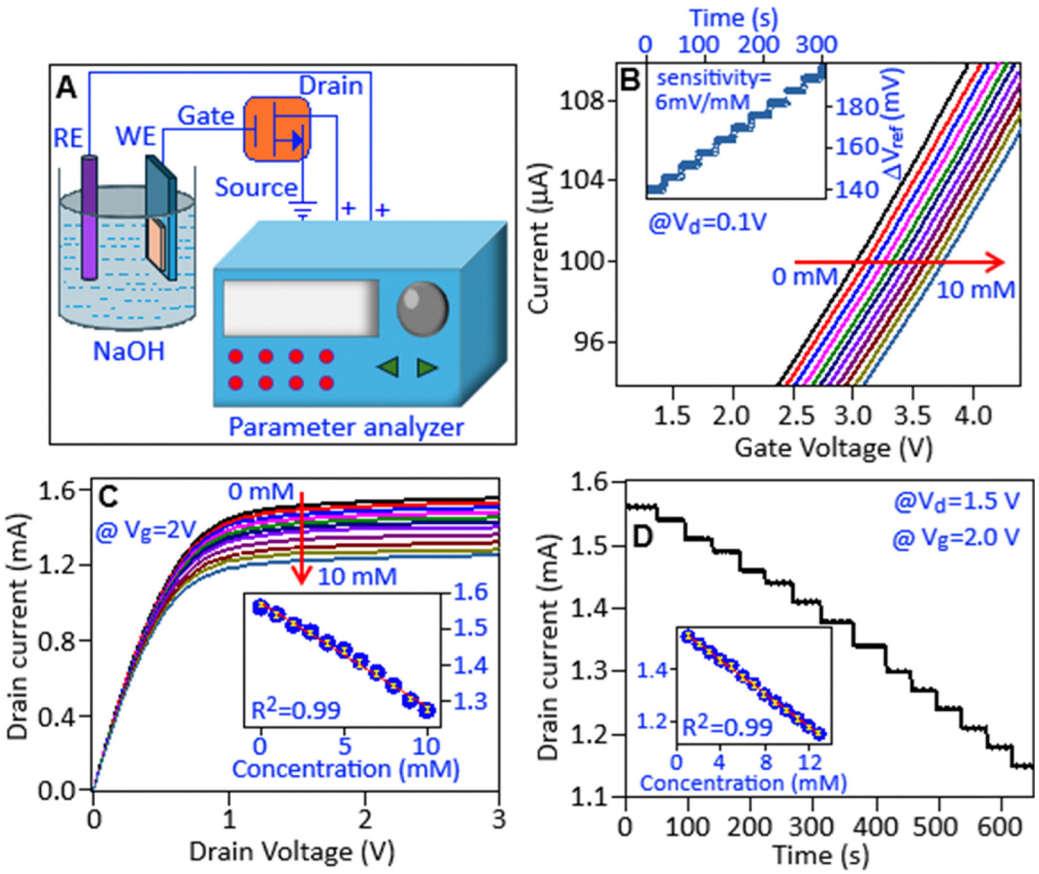

Fig. 6 (A) Schematic representation of the extended-gate field-effect transistor based sensor. (B) Transfer characteristics of the sensor with increasing glucose concentrations (0–10 mM) at a constant drain voltage of 0.1 V. The inset demonstrates stepwise change in potential difference between the working and reference electrodes. (C) Output characteristics of the sensor at a fixed gate voltage of 2.0 V with increasing glucose concentrations. The inset shows the relationship between drain current and glucose concentration (the test was repeated 5 times). (D) Real-time drain current response of the sensor upon sequential addition of glucose (0–14 mM) at constant gate and drain voltages. The inset shows a linear relationship between drain current and glucose concentration (the test was repeated 5 times).

indicating a modulation of the effective gate potential by the glucose–electrode interaction.[45–48] This shift, corresponding to a voltage sensitivity of 6 mV mM^{-1}, arises from changes in the potential between the reference and working electrodes, altering the effective gate-source voltage and reference voltage ($V_{eff} = V_{GS} - V_{ref}$). A stepwise change in potential difference between the working and reference electrodes was observed with glucose addition (Fig. 6B, inset). For $V_{DS} > V_{GS} - V_{th}$, the channel near the drain becomes pinched-off, and I_{DS} becomes largely independent of V_{DS}, primarily controlled by V_{GS}. Under these circumstances, the saturation current can be represented as given in eqn (6):

$$I_{Sat} = \mu \frac{W}{2L} C_{ox} (V_{GS} - V_{th})^2 \quad (6)$$

Output characteristics (I_{DS}–V_{DS}), measured at a fixed gate voltage (V_{GS}) of 2 V, showed a gradual decrease in current with glucose addition, Fig. 6C. This is attributed to the change in V_{ref} developing at the sensing interface, which opposes the applied gate voltage (V_{GS}), thereby reducing the V_{eff} and suppressing the drain current, particularly in the saturation region.[50] From these output curves, a current sensitivity of 0.03 mA mM^{-1} cm^{-2} and an LOD of 0.61 mM were estimated with an R^2 value of 0.99 (inset of Fig. 6C). Finally, real-time performance was assessed *via* the study of I_{DS} at a constant V_{GS} (2.0 V) and V_{DS} (1.5 V), Fig. 6D. The drain current (I_{DS}) systematically decreased upon sequential glucose addition (0 to 14 mM), consistent with the modulation of the effective gate potential observed previously. This method yielded excellent linearity ($R^2 \sim 0.99$, Fig. 6D, inset), a sensitivity of 0.033 mA mM^{-1} cm^{-2} and an LOD of 0.28 mM, highlighting the potential advantages of fixed-bias operation for response time and stability.

The selectivity of the PCFC-modified ITO electrode using an EGFET system was determined in the presence of glucose and common biological interferents like dopamine, epinephrine, sucrose and cholesterol, Fig. 7A. The results demonstrated preferential detection of glucose (5 mM), yielding a significant current change (ΔI_{DS}) compared to the current responses produced by the interfering species. A key aspect of reliability of the sensor is reproducibility, which was tested by preparing ten individual electrodes and measuring their response towards glucose at a concentration of 3 mM, Fig. 7B. The data revealed high stability and repeatability of the electrodes, quantified by a standard deviation of 3.47%. This level of consistency supports the viability for practical use of the sensor. The reusability study represents a critical and practical aspect of sensor deployment, directly impacting its long-term performance and cost-efficiency. The reusability performance of the PCFC-modified ITO electrode demonstrated notable limitations, as evidenced by a progressive increase in voltage change with successive cycles of use, Fig. 7C. Potential reasons for this degradation include charge density changes on the working electrode due to glucose ion adsorption and physical damage like micro-cracking in the deposited film resulting

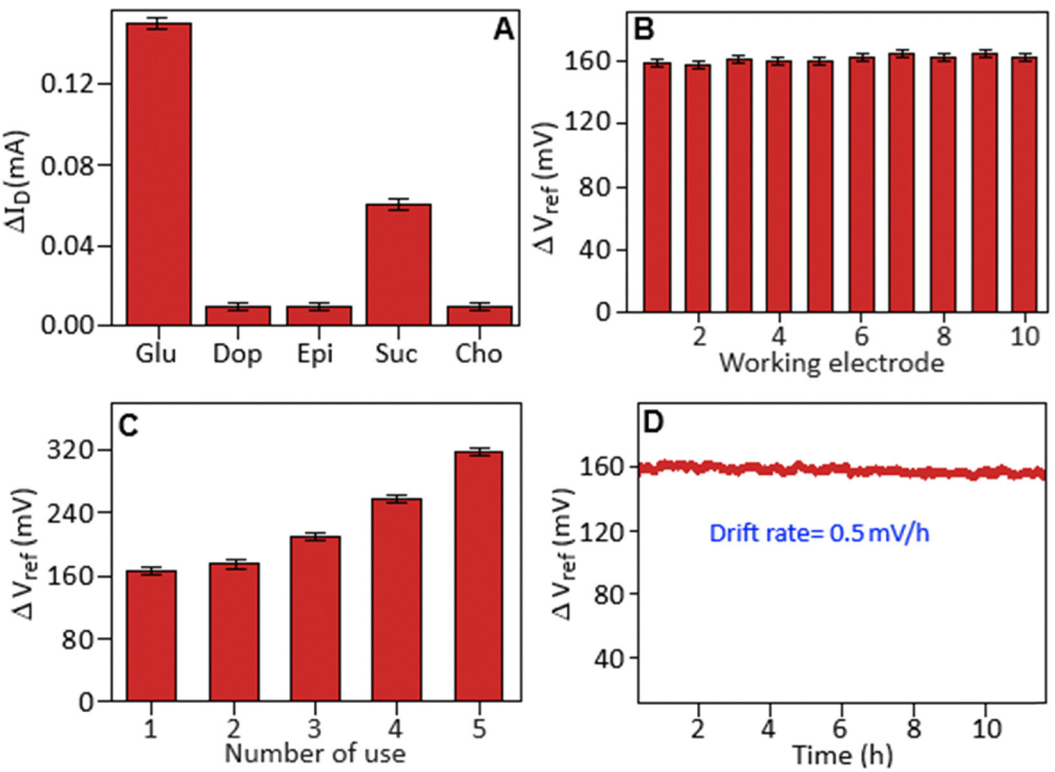

Fig. 7 (A) Selectivity study of glucose (Glu), dopamine (Dop), epinephrine (Epi), sucrose (Suc) and cholesterol (Cho) using an EGFET system with a PCFC-modified ITO electrode. (B) Reproducibility of the sensor tested with ten PCFC-modified ITO electrodes. (C) Reusability performance of the PCFC-modified ITO electrode over five successive cycles. (D) Long-term stability of the sensor evaluated by monitoring voltage drift for a period of 11 hours.

Table 1 Analysis of glucose detection in Fusayama/Meyer artificial saliva solution spiked with different concentrations of glucose

Sample	Added (mM)	Found (mM)	Relative error (%)	RSD (%) (3 measurements)	Recovery (%)
Fusayama/Meyer artificial saliva-glucose solution	0.50	0.51	2.00	0.29	102.00
	2.00	2.12	6.00	0.27	106.00
	4.00	4.21	5.25	0.26	105.25

from repeated wet-and-dry cycles. Improving both the surface chemistry and mechanical robustness is therefore necessary to enhance the reusability of the electrode. Finally, long-term stability was evaluated by monitoring voltage drift, the gradual change in baseline signal over time. Minimal drift is crucial for accurate, extended measurements. The sensor exhibited a minimal drift rate of 0.5 mV/h for a period of 11 hours, Fig. 7D. This indicates high intrinsic stability and reliable performance, suggesting that the sensor maintains its calibration well over time. The PCFC-based EGFET sensor demonstrated a level of performance that is highly comparable with several recently reported nonenzymatic glucose sensors, as summarized in Table S1.

3.3. Real sample analysis

The practical performance of the PCFC-modified ITO electrode was assessed using an EGFET-based sensor in the presence of commercially available Fusayama/Meyer artificial saliva solution. Upon spiking the saliva with glucose concentrations of 0.5, 2.0 and 4.0 mM, the change in drain current was observed. The corresponding estimated recoveries were obtained, ranging from 102.00 to 106.00%, with relative errors below 6% and relative standard deviation (RSD) below 0.3% (n = 3), as summarized in Table 1. These results demonstrate the high accuracy and repeatability of the sensor under physiologically relevant conditions, highlighting its suitability for glucose detection.

4. Conclusion

Organic molecule-stabilized nanostructured potassium copper ferrocyanide with a face-centered cubic structure was synthesized *via* a complexation-mediated approach and characterized using optical, structural and microscopic techniques. The potassium copper ferrocyanide-based electrochemical glucose sensor demonstrated excellent analytical performance, as evidenced by its high sensitivities in both cyclic voltammetry and differential pulse voltammetry, measured to be 0.41 mA mM^{-1} cm^{-2} and 0.50 mA mM^{-1} cm^{-2}, respectively. The corresponding limits of detection were determined to be 1.09 mM for CV and 1.01 mM for DPV, indicating reliable low-level glucose detection capability. Furthermore, the sensor exhibited good operational stability and reproducibility, which can be attributed to the reversible redox behavior of the Cu^{2+}/Cu^{3+} redox couple in alkaline media. The successful application of the sensor in artificial saliva samples further confirmed the strong potential of the PCFC-based FET sensor for accurate and repeatable glucose detection in complex biological fluids. Even in the presence of various interfering species typically found in such matrices, the sensor maintained stable and reliable performance, demonstrating its robustness for practical use. It achieved a sensitivity of 0.033 mA mM^{-1} cm^{-2} and a low detection limit of 0.28 mM, highlighting its capability to detect physiologically relevant glucose concentrations with high precision. The findings of this study suggest that hexane-1,6-diamine stabilized potassium copper ferrocyanide is a promising active material for the development of high-performance non-enzymatic electrochemical and EGFET-based glucose sensors, thereby contributing to glucose monitoring and personalized healthcare.

Author contributions

CS: conceptualization, validation, draft writing, investigation, material characterization and data acquisition. PK: material synthesis and characterization. MH: material synthesis and investigation. KM: conceptualization, resources, supervision and writing.

Conflicts of interest

The authors declare no conflict of interest.

Data availability

Data will be made available on request.

The data supporting this article have been included as part of the supplementary information (SI). Supplementary information is available. See DOI: https://doi.org/10.1039/d5ma01041a.

Acknowledgements

This study was supported by the Faculty of Science, University Research Council and the Global Excellence and Stature program 4.0, University of Johannesburg.

References

1 H. Lee, Y. Hong, S. Baik, T. Hyeon and D. Kim, *Adv. Healthcare Mater.*, 2018, **7**, 1–14.
2 H. Zhu, L. Li, W. Zhou, Z. Shao and X. Chen, *J. Mater. Chem. B*, 2016, **4**, 7333–7349.
3 D. Zhai, B. Liu, Y. Shi, L. Pan, Y. Wang, W. Li, R. Zhang and G. Yu, *ACS Nano*, 2013, **7**, 3540–3546.
4 I. Ahmed, N. Jiang, X. Shao, M. Elsherif, F. Alam, A. Salih, H. Butt and A. Yetisen, *Sens. Diagn.*, 2022, **1**, 1098–1125.

5 M. Wei, Y. Qiao, H. Zhao, J. Liang, T. Li, Y. Luo, S. Lu, X. Shi, W. Lu and X. Sun, *Chem. Commun.*, 2020, **56**, 14553–14569.
6 F. Soltanian, M. Nosrati, S. Mobayen, C. Li, T. Pan, M. Ke and P. Skruch, *Sci. Rep.*, 2023, **13**, 17527.
7 A. T. Lawal, *Biosens. Bioelectron.*, 2018, **106**, 149–178.
8 Z. Li, Y. Chen, Y. Xin and Z. Zhang, *Sci. Rep.*, 2015, **5**, 16115.
9 M. Wooten, S. Karra, M. Zhang and W. Gorski, *Anal. Chem.*, 2014, **86**, 752–757.
10 R. Sheldon and S. van Pelt, *Chem. Soc. Rev.*, 2013, **42**, 6223–6235.
11 J. Tang, Y. Wang, J. Li, P. Da, J. Genga and G. Zheng, *J. Mater. Chem. A*, 2014, **2**, 6153–6157.
12 N. Myeni, V. Perla, S. Ghosh and K. Mallick, *Mater. Today Commun.*, 2020, **25**, 101291.
13 M. Choudhary, S. Shukla, A. Taher, S. Siwal and K. Mallick, *ACS Sustainable Chem. Eng.*, 2014, **2**, 2852–2858.
14 X. You and J. Pak, *Sens. Actuators, B*, 2014, **202**, 1357–1365.
15 R. Adzhri, M. Arshad, S. Gopinath, A. Ruslinda, M. Fathil, R. Ayub, M. Nor and C. Voon, *Anal. Chim. Acta*, 2016, **917**, 1–18.
16 T. Nguyen, C. Nguyen, M. Huynh, H. Vu, T. Nguyen and N. Nguyen, *J. Nanobiotechnol.*, 2023, **21**, 411.
17 S. Nemati, G. Dehghan, N. Sheibani and Y. Abdi, *IEEE Sens. J.*, 2024, **24**, 17324–17336.
18 S. Cao, P. Sun, G. Xiao, Q. Tang, X. Sun, H. Zhao, S. Zhao, H. Lu and Z. Yue, *Electrochem. Sci. Adv.*, 2022, **3**, e2100207.
19 S. Sinha, T. Pal, D. Kumar, R. Sharma, D. Kharbanda, P. K. Khanna and R. Mukhiya, *Mater. Lett.*, 2021, **304**, 130556.
20 S. Zhao, C. Shi, H. Hu, Z. Li, G. Xiao, Q. Yang, P. Sun, L. Cheng, W. Niu, J. Bi and Z. Yue, *Biosens. Bioelectron.*, 2019, **151**, 111962.
21 C. Hu, M. Al-Rawhani, B. Cheah, S. Velugotla and D. Cumming, *IEEE Sens. J.*, 2018, **18**, 484–493.
22 J. Qi, H. Zhang, Z. Ji, M. Xu and Y. Zhang, *Appl. Phys. A: Mater. Sci. Process.*, 2015, **119**, 807–811.
23 P. Ni, Y. Sun, Y. Shi, H. Dai, J. Hu, Y. Wang and Z. Li, *RSC Adv.*, 2014, **4**, 28842–28847.
24 W. Huang, S. Ding, Y. Chen, W. Hao, X. Lai, J. Peng, J. Tu, Y. Cao and X. Li, *Sci. Rep.*, 2017, **7**, 1–11.
25 L. Wang, Y. Zhang, Y. Xie, J. Yu, H. Yang, L. Miao and Y. Song, *Appl. Surf. Sci.*, 2017, **402**, 47–52.
26 Z. Wang, X. Yuan, S. Cong, Z. Chen, Q. Li, F. Geng and Z. Zhao, *ACS Appl. Mater. Interfaces*, 2018, **10**, 15065–15072.
27 Y. Zong, Y. Zhang, X. Lin, D. Ye, D. Qiao and S. Zeng, *RSC Adv.*, 2017, **7**, 31352–31364.
28 F. Song, L. Bai, A. Moysiadou, S. Lee, C. Hu, L. Liardet and X. Hu, *J. Am. Chem. Soc.*, 2018, **140**, 7748–7759.
29 J. Olenik, V. Shvalya, M. Modic, J. Ekar, J. Kovač, U. Cvelbar and J. Walsh, *J. Anal. Test.*, 2023, **7**, 392–404.
30 B. Gangaja, S. Chandrasekharan, S. Vadukumpully, S. V. Nair and D. Santhanagopalan, *J. Power Sources*, 2016, **340**, 356–364.
31 J. P. Espinós, J. Morales, A. Barranco, A. Caballero, J. P. Holgado and A. R. González-Elipe, *J. Phys. Chem. B*, 2002, **106**, 6921–6929.
32 A. Gayathri, S. Mathi, M. Vijayarangan, J. Jayabharathi and V. Thanikachalam, *ChemistrySelect*, 2022, **7**, e202203616.
33 G. Kuntoji, N. Kousar, S. Gaddimath and L. Sannegowda, *Biosensor*, 2024, **14**, 277.
34 X. Wang, X. Dong, Y. Wen, C. Li, Q. Xiong and P. Chen, *Chem. Commun.*, 2012, **48**, 6490–6492.
35 Y. Zhang, F. Xu, Y. Sun, Y. Shi, Z. Wen and Z. Li, *J. Mater. Chem.*, 2011, **21**, 16949–16954.
36 T. Zhe, X. Sun, Y. Liu, Q. Wang, F. Li, T. Bu, P. Jia, Q. Lu, J. Wang and L. Wang, *Microchem. J.*, 2019, **151**, 104197.
37 K. Tian, M. Prestgard and A. Tiwari, *Mater. Sci. Eng., C*, 2014, **41**, 100–118.
38 J. Lee, H. Kong, H. Kim, S. Ko, J. Mun and J. Yeo, *ACS Appl. Electron. Mater.*, 2024, **6**, 1274–1282.
39 X. Cheng, J. Zhang, H. Chang, L. Luo, F. Nie and X. Feng, *J. Mater. Chem. B*, 2016, **4**, 4652–4656.
40 S. Baek, J. Roh, C. Park, M. Kim, R. Shi, S. Kailasa and T. Park, *Mater. Sci. Eng., C*, 2020, **107**, 110273.
41 P. Viswanathan, J. Park, D. Kang and J. Hong, *Colloids Surf., A*, 2019, **580**, 123689.
42 S. Sheibani, L. Capua, S. Kamaei, S. S. A. Akbari, J. Zhang, H. Guerin and A. M. Ionescu, *Commun. Mater.*, 2021, **1**, 1–10.
43 L. Shi, L. Gong, Y. Wang, Y. Li and Y. Zhang, *Sens. Actuators, B*, 2023, **400**, 134944.
44 J. Jeon and W. Cho, *Sci. Technol. Adv. Mater.*, 2020, **21**, 371–378.
45 K. Shibata and A. Nakamura, *SN Appl. Sci.*, 2022, **4**, 253.
46 A. Mishra, D. Jarwal, B. Mukherjee, A. Kumar, S. Ratan and S. Jit, *IEEE Sens. J.*, 2020, **20**, 5039–5047.
47 A. Mishra, D. Jarwal, B. Mukherjee and S. Jit, *IEEE Trans Nanobioscience*, 2021, **21**, 3–9.
48 M. Das, T. Chakraborty, C. Y. Lin, R. Lin and C. Kao, *Mater. Chem. Phys.*, 2021, **278**, 125652.
49 A. Singh, A. Pandey and P. Chakrabarti, *IEEE Sens. J.*, 2020, **21**, 5779–5786.
50 A. Vinukumar, M. Matada, G. P. Kuppuswamy, S. Jayan, K. Vivek, S. Jayaraman, Y. Sivalingam, N. Tocci, A. Ganesan and L. Conterno, *ACS Appl. Mater. Interfaces*, 2024, **16**, 53405–53418.